Moment-method calculations on multiple apertures using singular basis functions

Andersson, Tommy

1991

CODEN:LUTEDX/(TEAT-7017)/1-29/(1991)

Revision No. 1: February, 1993

Moment-method calculations on multiple apertures using singular basis functions

Tommy Andersson

Department of Electroscience
Electromagnetic Theory
Lund Institute of Technology
Sweden

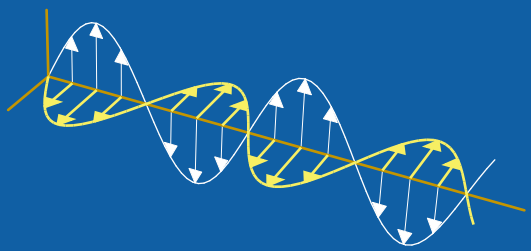

Tommy Andersson

Department of Electromagnetic Theory
Lund Institute of Technology
P.O. Box 118
SE-221 00 Lund
Sweden

Editor: Gerhard Kristensson

Abstract

The transmission properties of perforated perfectly conducting screens are of practical interest. The treatment of non-periodical structures by numerical techniques, such as the method of moments, is very computer intensive. In this paper it is shown that using well adapted basis functions, the number of unknowns can be drastically reduced. Advantages and limitations of the method are discussed. Numerical results are presented illustrating transmission properties of arrays of square and rectangular apertures.

1 Introduction

Perforated metallic screens and wire mesh screens are often used for electromagnetic shielding and filtering purposes. The reflection and transmission properties of infinite wire grids and periodically apertured screens have been analyzed by many authors in the past, e.g., [1]-[4]. However, the treatment of finite structures is also of practical interest. During the last decades different numerical methods, such as the method of moments (MoM) [5], have been successfully applied to aperture problems [6], [7]. An attempt to apply the MoM to an array of apertures, constituting one wire mesh covered aperture, was made in Ref. [8]. Truncated period structures have been considered by, e.g., [9] and [10]. Recursive schemes have recently been suggested to handle finite, non-periodic structures [11], [12].

However, the performance of numerical methods seems to depend heavily on the ability to handle the singular behaviour of the fields near the rims of the apertures. The MoM involves the expansion of the unknown function in terms of a set of basis functions. Basis functions with correct edge behaviour have successfully been used to calculate the polarizability of electrically small apertures [13], [14]. Recently, the scattering by a thin conducting square plate was treated by the author [15]. Basis functions with correct edge and corner singularities were used, giving greatly enhanced convergence. Here, this approach is applied to calculate the transmission properties of an array of rectangular apertures in an infinite, thin, perfectly conducting screen.

In Section 2 the integral equation, the MoM approach and the basis functions are briefly described. Some relevant transmission quantities are defined in Section 3. In Section 4 numerical results are presented. The enhanced convergence, due to the singular basis function, is illustrated and the limitations of the method are discussed. The transmission coefficients and transmission cross sections are calculated for different geometries varying the distance between the apertures. Finally, some conclusions are given in Section 5.

2 Integral equation and MoM approach

The diffracted electromagnetic field through apertures in a perfectly conducting, thin, plane screen can, according to Babinet's principle, be found by solving the complementary problem, i.e., the electromagnetic scattering by perfectly conducting plates in free space replacing the apertures. However, in this paper we adopt the well known formulation using the equivalence principle and magnetic sources, i.e., the solution is expressed in terms of the equivalent magnetic sources in the apertures [6], [7],

[16]. In this section an integral equation is formulated and the method of moments is applied.

The integral equation

Let the screen be located in the x-y- plane in a Cartesian coordinate system, cf. Fig. 1a. The surrounding homogeneous media is characterized by the permeability μ and the permittivity ε. The sources are assumed to be located in the half space $z < 0$, while the half space $z > 0$ is source free. Denote by $\boldsymbol{H}^{in}$ the magnetic field of the incident wave in the absence of the screen. A harmonic time dependence is assumed and the time factor $e^{-i\omega t}$ is suppressed everywhere.

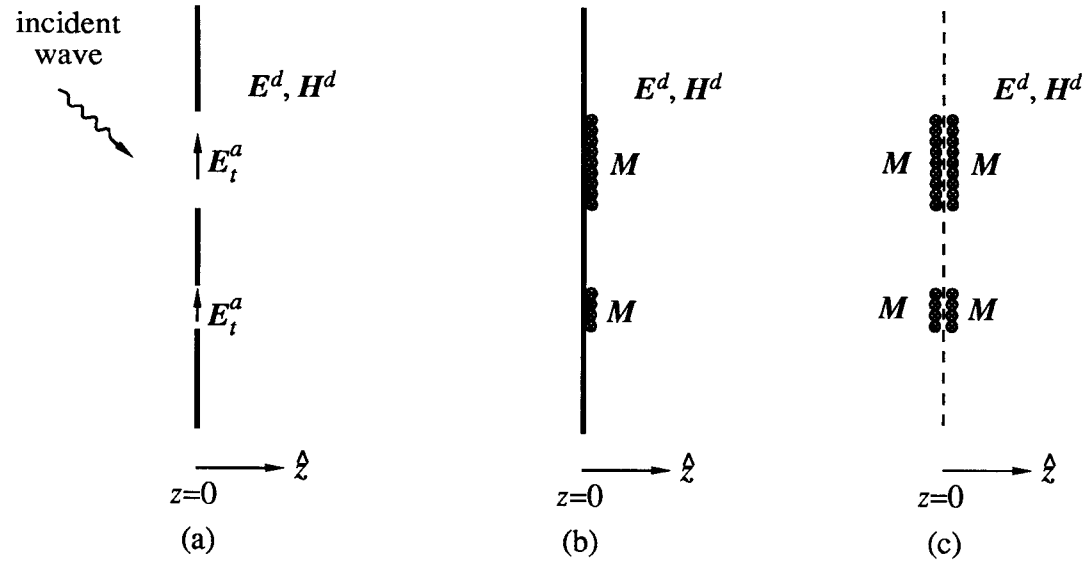

Fig. 1. The original aperture configuration (a) and the equivalent half spaces z>0 (b) and (c).

The diffracted electromagnetic field $\boldsymbol{E}^d$, $\boldsymbol{H}^d$ in the half space $z > 0$ is determined by the tangential electric field $\boldsymbol{E}_t^a$ in the apertures. The equivalence principle [17] implies that the original aperture configuration can be replaced by a perfectly conducting screen and a magnetic surface current $\boldsymbol{M}$ that generates the electric field $\boldsymbol{E}_t^a$, cf. Fig. 1b. $\boldsymbol{M}$ is placed over the short-circuited aperture regions and

$$\boldsymbol{M} = -\hat{\boldsymbol{z}} \times \boldsymbol{E}_t^a \tag{1}$$

The method of image implies that the fields in the half space $z > 0$ can be expressed as if they were generated by a magnetic surface current $2\boldsymbol{M}$ in free space, cf. Fig. 1c.
Hence, the diffracted magnetic field $\boldsymbol{H}^d$ can be expressed as

$$\boldsymbol{H}^d = -\nabla\Phi + i\omega\boldsymbol{F} \tag{2}$$

where the magnetic scalar potential Φ and the electric vector potential $\boldsymbol{F}$ are given by

$$\Phi(\boldsymbol{r}) = \frac{1}{\mu} \int_S 2m(\boldsymbol{r}')\, G(\boldsymbol{r},\boldsymbol{r}')\, \mathrm{d}S' \tag{3}$$

and

$$\boldsymbol{F}(\boldsymbol{r}) = \varepsilon \int_S 2\boldsymbol{M}(\boldsymbol{r}')\, G(\boldsymbol{r},\boldsymbol{r}')\, \mathrm{d}S' \tag{4}$$

respectively.
Here S is the surface of the apertures in the screen. The magnetic surface charge density m is related to surface divergence of $\boldsymbol{M}$ through the equation of continuity,

$$m = \frac{\nabla_S \cdot \boldsymbol{M}}{i\omega} \tag{5}$$

The surface divergence $\nabla_S \cdot \boldsymbol{M}$ is here $\partial_x M_x + \partial_y M_y$ since S is a surface in the x-y-plane. The free space Green function $G(\boldsymbol{r},\boldsymbol{r}')$ is defined as

$$G(\boldsymbol{r},\boldsymbol{r}') = \frac{\mathrm{e}^{ik|\boldsymbol{r}-\boldsymbol{r}'|}}{4\pi|\boldsymbol{r}-\boldsymbol{r}'|} \tag{6}$$

where the wave number $k = \omega\sqrt{\mu\varepsilon} = 2\pi/\lambda$.
The geometry of the original configuration implies that the induced currents on the conducting surface of the screen produce no tangential magnetic field in the aperture regions. Hence, the tangential magnetic field in the apertures is not changed due to the presence of the screen. An integral equation can now be formulated as

$$\hat{\boldsymbol{z}} \times (-\nabla\Phi + i\omega\boldsymbol{F}) = \hat{\boldsymbol{z}} \times \boldsymbol{H}^{in}, \quad \boldsymbol{r} \text{ on } S \tag{7}$$

where Φ and $\boldsymbol{F}$ are given by Eqs. (3) and (4), $\boldsymbol{H}^{in}$ is the magnetic field of the incident wave and S is the surface of the apertures.
Notice that the limits on the left-hand side of Eq. (7) are well-defined quantities, since $\boldsymbol{F}(\boldsymbol{r})$ and the tangential derivatives $\hat{\boldsymbol{z}} \times \nabla\Phi$ are continuous on the surface S. The mathematical details of these limits can be found in, e.g., [18].
This integral equation is mathematically identical to the one obtained in Ref. [15] solving the complementary scattering problem, hence the same numerical solution method can be applied. A short outline of this approach is given below. The reader interested in more details is referred to Ref. [15].

The matrix equation

The MoM is applied to Eq. (7) and an approximation of the integral equation is obtained. The magnetic surface current $\boldsymbol{M}$ and the magnetic surface charge m are expanded in terms of a set of vector basis functions f_p with unknown coefficients a_p, i.e.,

$$\boldsymbol{M} = \sum_p a_p f_p \tag{8}$$

$$m = \frac{1}{i\omega} \sum_p a_p\, \nabla_S \cdot f_p \tag{9}$$

Let w_q be a set of testing functions tangential to the surface S and define a symmetric product as

$$\langle f, g \rangle = \int_S f \cdot g \, dS \tag{10}$$

Testing of Eq. (7) yields

$$- \langle \nabla \Phi, w_q \rangle + i\omega \langle F, w_q \rangle = \langle H^{in}, w_q \rangle \tag{11}$$

Choose the testing functions w_q such that

$$w_q \cdot \hat{n}_L = 0 \text{ on } L \tag{12}$$

where L is the boundary of S and $\hat{n}_L$ is the outward pointing unit normal to L. This property of w_q implies [15]

$$\langle \nabla \Phi, w_q \rangle = - \int_S \Phi \, \nabla_S \cdot w_q \, dS \tag{13}$$

The matrix equation can now be explicitly expressed as

$$\sum_p a_p \int_S \int_S (\nabla_S \cdot f_p(r') \, \nabla_S \cdot w_q(r) - k^2 f_p(r') \cdot w_q(r)) \, G(r,r') \, dS' dS =$$
$$= \frac{i\omega\mu}{2} \int_S H^{in}(r) \cdot w_q(r) \, dS \qquad q = 1,2,3... \tag{14}$$

where $k^2 = \omega^2 \varepsilon u$.

Basis functions

In Ref. [15] the scattering by a perfectly conducting square plate is calculated. At the edges and corners of a thin, perfectly conducting plate the fields and source distributions have known singular behaviour, see, e.g., [19]. It is shown in Ref. [15] that the use of basis functions with correct edge and corner behaviour greatly enhance the convergence of the scattering problem compared to the use of ordinary "rooftop" functions.

The aperture problem, as it is formulated in this paper, leads to an equation and to singular behaviour of the fields that are similar to the scattering problem [15]. As a consequence of that, the singular basis functions used in Ref. [15] can be used also in this aperture problem. We give here just a short description of these basis functions, for more details cf. [15].

Subdomain basis functions are used, i.e., basis functions with support only in subsections of the domain. To assure continuity of the magnetic current density in the direction of flow an overlapping technique is used. This prevents fictitious magnetic line charges at the boundaries of the subsections.

In the interior of the domain the current is approximated by ordinary rooftop basis functions, cf. Fig. 2.

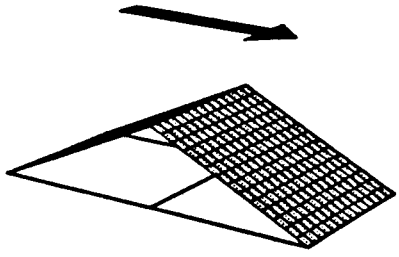

Fig. 2. The interior basis functions. The magnetic current is approximated by rooftop functions.

At the edges two kinds of basis functions are used, cf. Fig. 3. The magnetic surface current tangential to an edge is expanded in basis functions with the singularity $1/\sqrt{d}$, where d represents the perpendicular distance to the edge, but have rooftop character in the direction of flow. The current flowing perpendicular to the edge is approximated by basis functions that go to zero as $\sqrt{d}$ near the edge, which agrees with the singularity $1/\sqrt{d}$ for the magnetic charge.

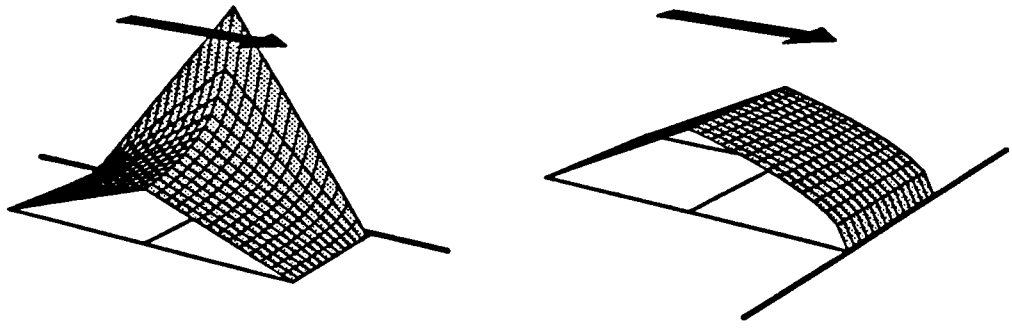

(a) (b)

Fig. 3. The basis functions used to approximate the magnetic current tangential (a) and perpendicular (b) to an edge.

At the corners the electric and magnetic fields have different singular behaviour. We use two kinds of basis functions corresponding to these two singularities.
The first kind is used to expand the magnetic current flowing in the radial direction towards the corner. The singularity of the related accumulated magnetic charge density $r^{\nu-1}$ corresponds to the singular behaviour of the magnetic field. Here r denotes the distance to the corner and the approximate value ν=0.30 according to [19]. The x and y components of these magnetic current basis functions are shown in Fig. 4. Note the correct edge behaviour and the linear parts used to connect the corner subsection with the adjacent edge subsections.

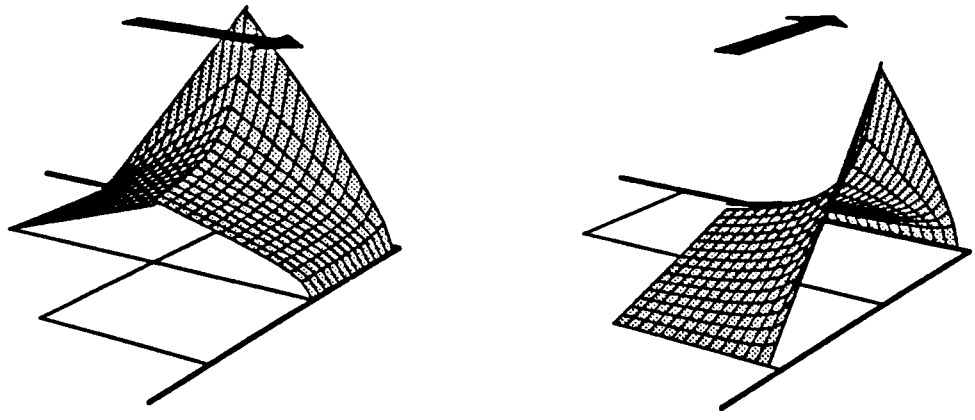

(a) (b)

Fig. 4. The corner basis functions used to obtain the correct magnetic singularity. The Cartesian components of the basis functions for the radial magnetic current are illustrated.

The second kind of corner basis functions expands the tangential magnetic current near the corner. This current has the same singularity as the electric field, $r^{\tau-1}$. The approximate value of the exponent is given by Ref. [19] as τ=0.82. Besides the correct corner and edge behaviour these basis functions are also solenoidal. Hence, no magnetic charge is accumulated which otherwise would influence the expansion of the magnetic field. The tangential current basis functions are illustrated in Fig. 5. The discontinuity of the current density that can be seen in Fig. 5 is due to computational considerations, cf. [15].

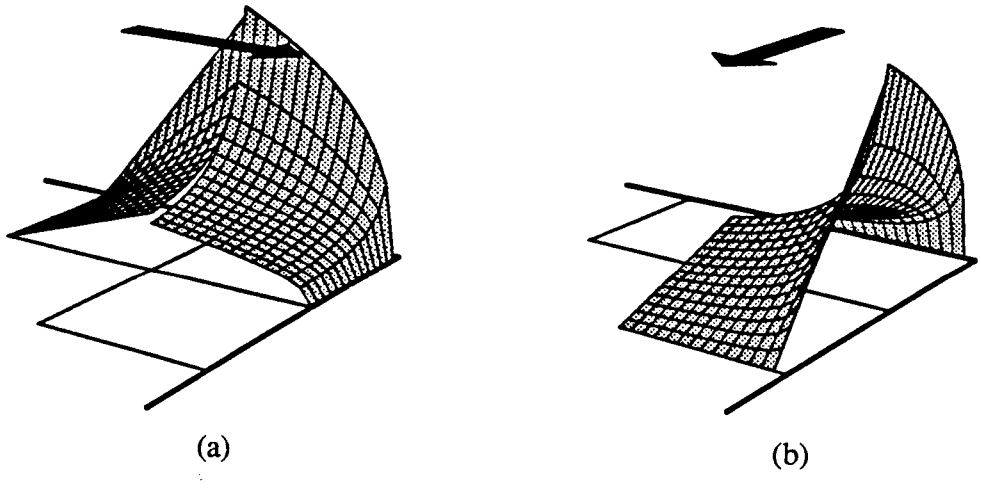

(a) (b)

Fig. 5. The corner basis functions used to obtain the correct electric singularity. The Cartesian components of the basis functions for the tangential magnetic current are illustrated.

Testing functions

We use Galerkin's method, i.e., the testing functions are identical to the basis functions. This is possible as the above described basis functions fulfil the requirements for the testing functions specified by Eq. (12).

Numerical treatment of the matrix equation

The use of complicated basis and testing functions like those described above, makes it essential to find numerically efficient methods to calculate the matrix elements given by Eq.(14). A multipole expansion technique to calculate the non self-patch terms of the matrix elements is described by the author in Refs. [15] and [20]. The translation properties of the spherical scalar wave functions [21] imply that the matrix elements can be expressed as a series of multipole moments. Moreover, this technique can be used to calculate the right side of Eq. (14) and the diffracted field. This subject is, however, not pursued in the present paper. The reader is referred to the above mentioned references.

3 Transmission quantities

The far diffracted field and the transmission quantities are conveniently expressed in the following vector function $\boldsymbol{K}$

$$\boldsymbol{K}(\hat{\boldsymbol{r}}) = \hat{\boldsymbol{r}} \times \left(\int_S \boldsymbol{M}(\boldsymbol{r}')\ e^{-ik\hat{\boldsymbol{r}}\cdot\boldsymbol{r}'} \mathrm{d}S' \times \hat{\boldsymbol{r}} \right) \tag{15}$$

This vector function can easily be computed using the multipole technique, cf. [15].
It can be shown that the diffracted field, given by Eq. (2), can be expressed in the far zone as

$$\boldsymbol{H}^d(\boldsymbol{r}) = i\omega\varepsilon \frac{e^{ik|\boldsymbol{r}|}}{2\pi|\boldsymbol{r}|} \boldsymbol{K}(\hat{\boldsymbol{r}}) \tag{16}$$

In the following we consider plane wave incidence. Let the incident wave be specified by

$$\boldsymbol{H}^{in} = \boldsymbol{H}_0\, \mathrm{e}^{i\boldsymbol{k}\cdot\boldsymbol{r}} \tag{17}$$

where $\boldsymbol{H}_0$ is a constant complex vector, and which is the field in the absence of the screen.
We define the transmission cross section τ, cf. e.g. [6], as

$$\tau(\theta,\phi) = \lim_{r\to\infty} 2\pi r^2 \frac{|\boldsymbol{H}^d|^2}{|\boldsymbol{H}^{in}|^2} \tag{18}$$

where $\boldsymbol{H}^d$ is the diffracted field at the observation point (r,θ,ϕ) $(z>0)$.
Using Eq. (16), the transmission cross section τ can be expressed

$$\tau(\theta,\phi) = \frac{\omega^2 \varepsilon^2}{2\pi} \frac{|\boldsymbol{K}|^2}{|\boldsymbol{H}_0|^2} \tag{19}$$

We define the transmission coefficient T of an array of apertures as the ratio of the power transmitted through the apertures to the power incident on the apertures, cf. [17]. Hence, for the configuration given by Fig. 1a, we have

$$T = \frac{\mathrm{Re} \int_S (\boldsymbol{E}^d \times \boldsymbol{H}^{d^*}) \cdot \hat{\boldsymbol{z}} \, \mathrm{d}S}{\mathrm{Re} \int_S (\boldsymbol{E}^{in} \times \boldsymbol{H}^{in^*}) \cdot \hat{\boldsymbol{z}} \, \mathrm{d}S} \tag{20}$$

In this expression the numerator should be evaluated in the right half space, i.e., z=0+. Using Eqs. (1), (15), (17) and the continuity of the electric and magnetic fields in the apertures, one obtains

$$T = -\frac{\mathrm{Re}(\boldsymbol{K}(\hat{\boldsymbol{k}}) \cdot \boldsymbol{H}_0^*)}{\sqrt{\mu/\varepsilon} \, |\boldsymbol{H}_0|^2 \, S \, \hat{\boldsymbol{k}} \cdot \hat{\boldsymbol{z}}} \tag{21}$$

where S is the area of the apertures.

4 Numerical results

Convergence

To check the validity of the method we first study the convergence of the transmission coefficient T for a configuration consisting of two square apertures and normal incidence. The length of the side of each aperture is 0.1λ. The results are highly dependent on the polarization of the incident wave. We assume in the following that the apertures are placed in the x-y-plane along the x-axis.

When the incident magnetic field is polarized in the $\hat{\boldsymbol{y}}$-direction, the convergence is fairly independent of the distance between the plates, cf. Fig. 6a. At zero distance the transmission coefficient agrees completely with the transmission coefficient of a corresponding, single, rectangular aperture. The magnetic current distribution, which corresponds to the tangential electric field in the aperture, is illustrated in Fig. 7a. As the distance between the apertures vanishes, the singular behaviour of the magnetic current flowing along the adjacent rims of the two apertures should disappear. However, as seen in Fig. 7a, the singular source distributions prescribed by the basis functions cause nonphysical oscillations. Still, using singular basis functions the convergence of the transmission coefficient is, as seen from Fig. 6, greatly enhanced compare to the use of ordinary, linear basis functions.

A different situation arises when the incident magnetic field is polarized in the $\hat{\boldsymbol{x}}$-direction. When the apertures get close to each other the convergence becomes very slow, cf. Fig. 6b. This is due to the increasing edge singularities of the sources as the distance between the apertures decreases. The corresponding phenomenon has recently been reported in the literature when calculating scattering by strips [12]. This type of

phenomena is, however, not mentioned in Ref. [8] for an aperture with a wire grid. The magnetic current distribution is shown in Fig. 7b. Notice that the curves representing the distances d=0 and d=0.02a are not valid, since the convergence at these distances is to slow, while the other curves correspond to convergent solutions, cf. Fig. 6b. The current distribution of the limiting case, a single rectangular aperture, is also shown. Obviously, the slow convergence at small distances may cause misleading results.

We have also made some studies of the convergence of the transmission coefficient at higher frequency, a=0.5λ. The above described characteristics seem to remain, although less accentuated. It is conjectured that this is due to the decreased influence from the singular magnetic charge distribution at higher frequencies, cf. the term $\nabla_S \cdot f_p$ $\nabla_S \cdot w_q$ in Eq. (14). We therefore refrain from depicting this higher frequency case since the main features of the problem are illustrated at low frequency.

Numerical examples

The fast convergence achieved with the singular basis functions makes the described method well suited for calculating the transmission properties of arrays of apertures. As just a few unknowns are needed for each aperture to obtain reasonable accuracy, configurations with multiple apertures can be treated with limited computational effort. (All computations presented have been carried out on a Sun 3/80 work station).

Figs. 8-9 illustrate the variation of the transmission coefficient T as the distances between apertures, arranged in a row, are varied. In the computation each aperture was divided into 7×7 "sub-squares". Note that the transmission coefficient shows a small maximum for the transverse polarization, while it is a monotonic function for the parallel polarization at the lower frequency a=0.1λ.

In Figs. 10-17 a series of numerical computations of the transmission cross section is given for four apertures oriented along a line. Two different incident angles (normal and oblique) at both polarizations are depicted for two different frequencies (a=0.1λ and a=0.5λ),

Figs. 18-21 show transmission cross sections for a more complicated configuration consisting of six rectangular apertures. The size of each aperture is 0.5λ × 1λ and the distances between the apertures are 0.25λ. Both polarizations as well as normal and oblique incidence are illustrated. Notice the excellent convergence in all cases that are shown; especially Fig. 18 where even the most coarse discretization gives a good result.

5 Summery and conclusions

We have presented a moment method approach to calculate the transmission properties of arrays of rectangular apertures in a perfectly conducting screen. Basis functions with correct singular behaviour were used to enhance the convergence and thus reducing the necessary truncation size of the moment method matrix. Numerical results were presented illustrating the performance of the method.

The method is less suited when treating apertures very close to each other, due to the special singular behaviour of the sources in those cases. Thus, an attractive extension of the technique would be to incorporate this behaviour into the basis functions. Another approach, would be to combine the presented method with some recursive technique, and thus, possibly, further reduce the computational costs.

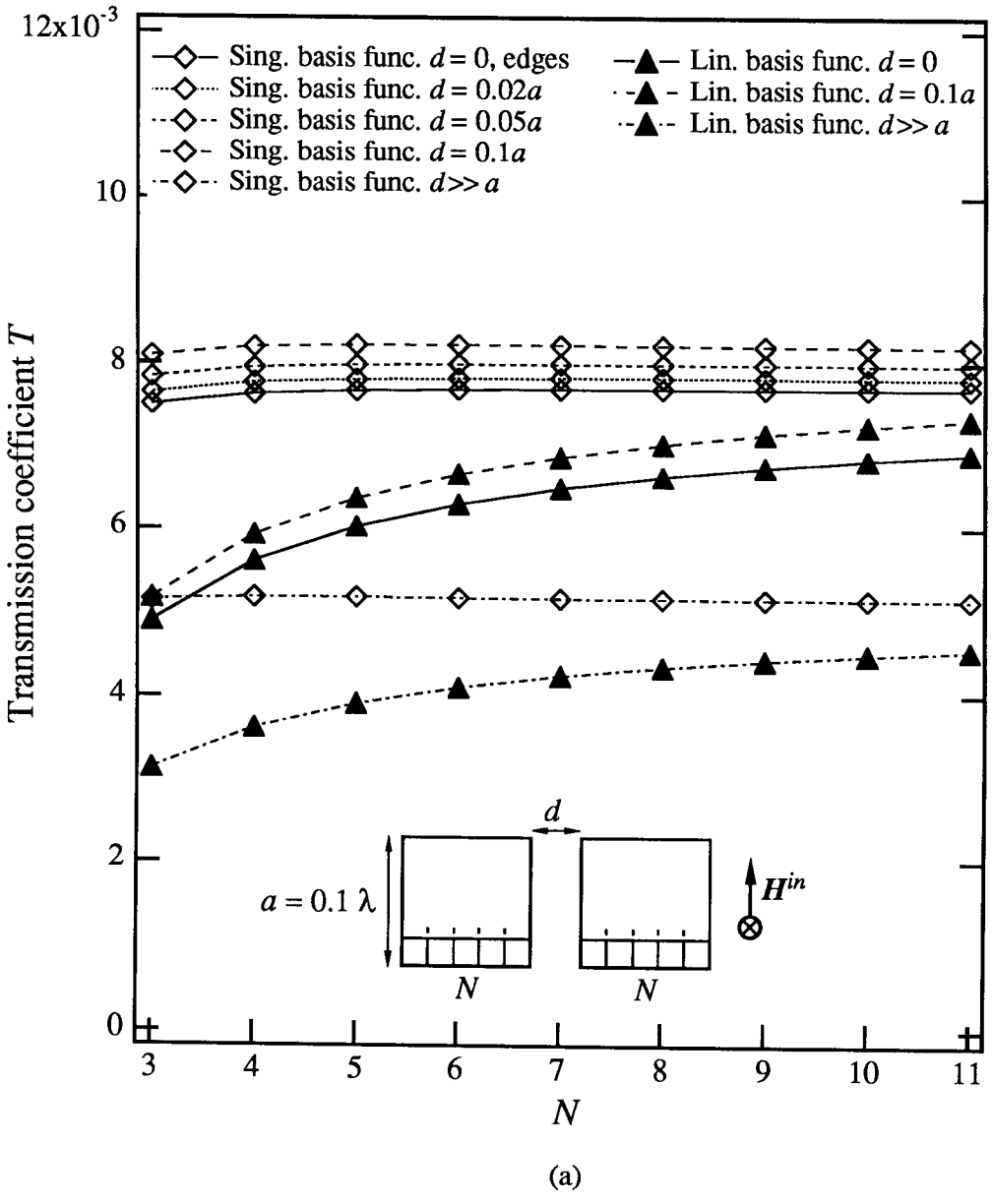

Fig. 6. Convergence of the transmission coefficient T for two square apertures, each with length of side a=0.1λ. Normal incidence. Each aperture is divided into $N \times N$ "sub-squares". The convergence is shown for different distances d between the apertures. The polarization of the incident magnetic field is (a) transverse / (b) parallel to the row of apertures.

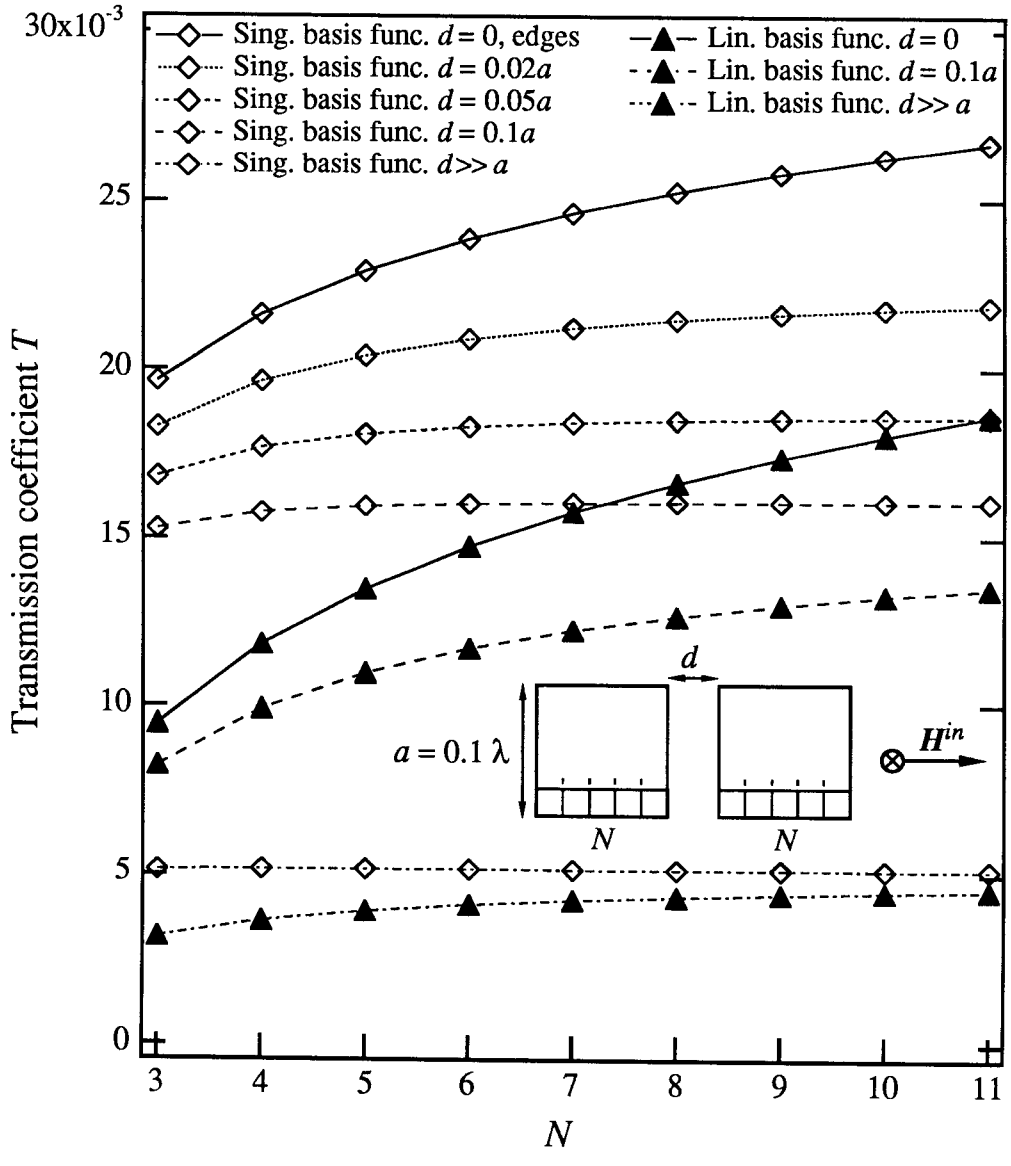

(b)

Fig. 6b. Caption, see Fig. 6a.

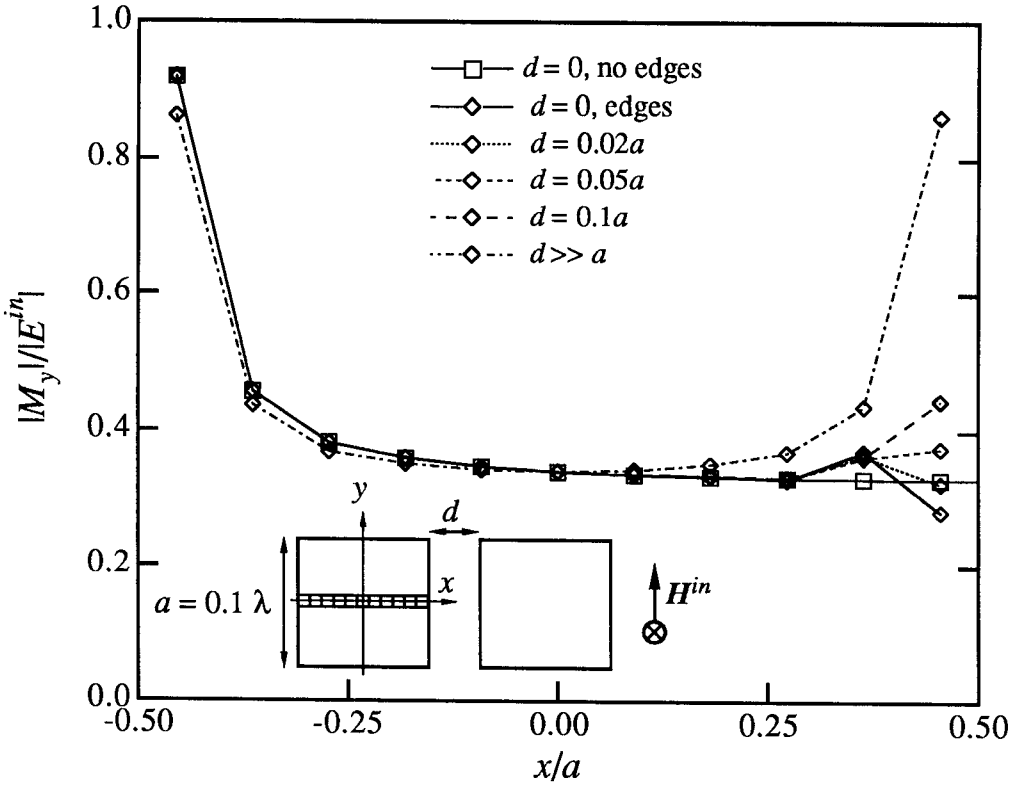

(a)

Fig. 7. The dominant component of the magnetic current density in one of two adjacent square apertures. Normal incidence. The mean values of the current density on "sub-squares" in the middle row parallel to the row of apertures are shown. The length of the side of each aperture is 0.1 λ. The apertures are divided into 11×11 "sub-squares". The polarization of the incident magnetic field is (a) transverse / (b) parallel to the row of apertures.

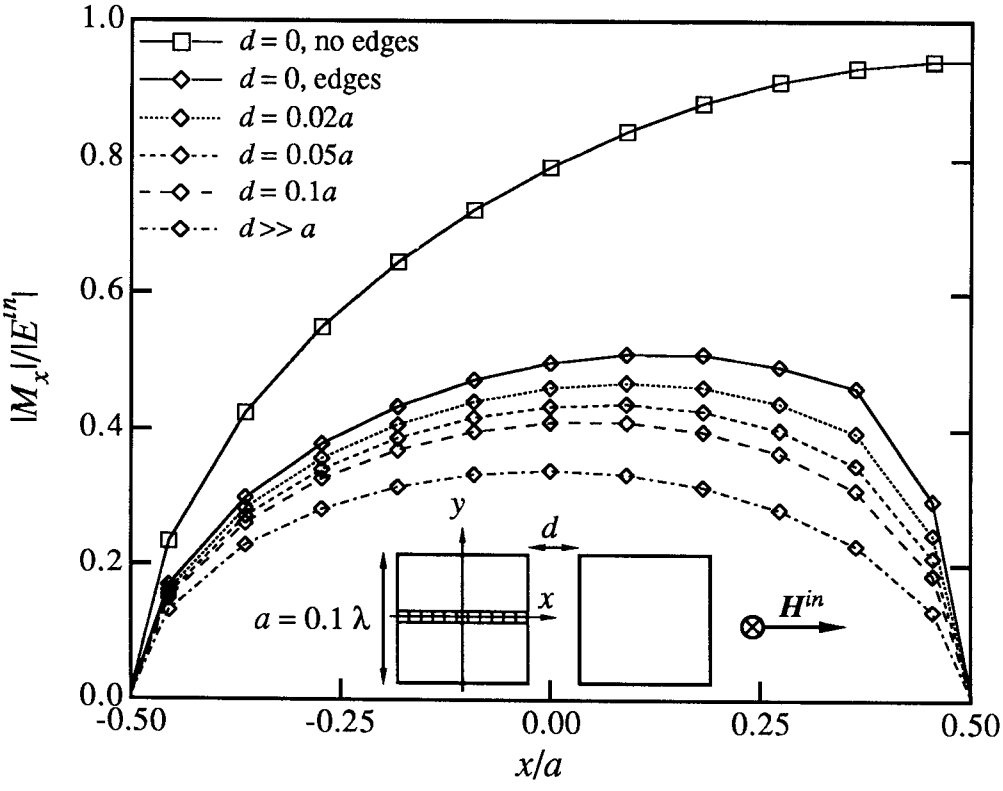

(b)

Fig. 7b. Caption, see Fig. 7a.

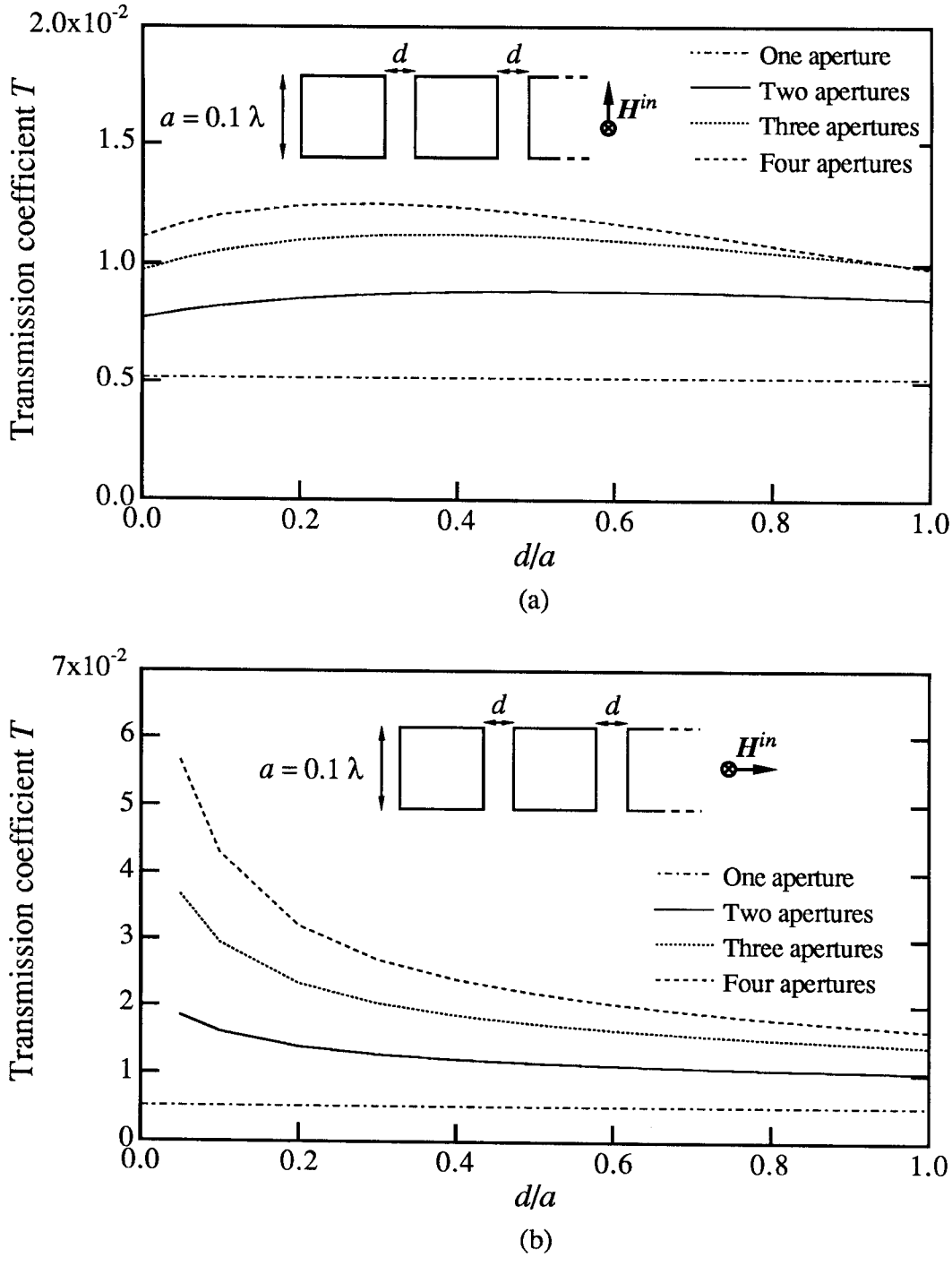

Fig. 8. The transmission coefficient for a row of square apertures versus the distance between the apertures. Normal incidence with the polarization of the magnetic field transverse (a) and parallel (b) to the row of apertures. The length of the side of each aperture is 0.1λ.

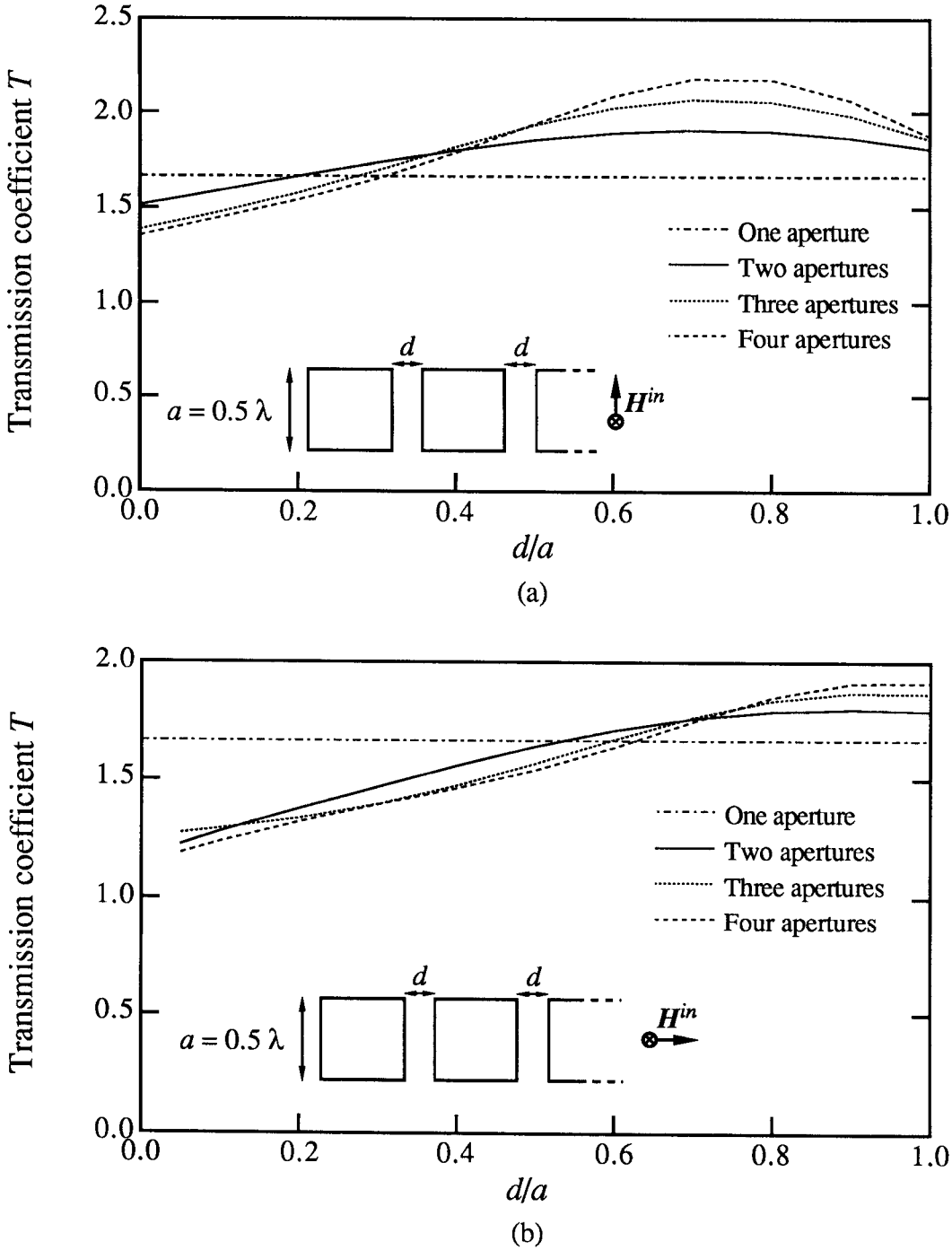

Fig. 9. The transmission coefficient for a row of square apertures versus the distance between the apertures. Normal incidence with the polarization of the magnetic field transverse (a) and parallel (b) to the row of apertures. The length of the side of each aperture is 0.5λ.

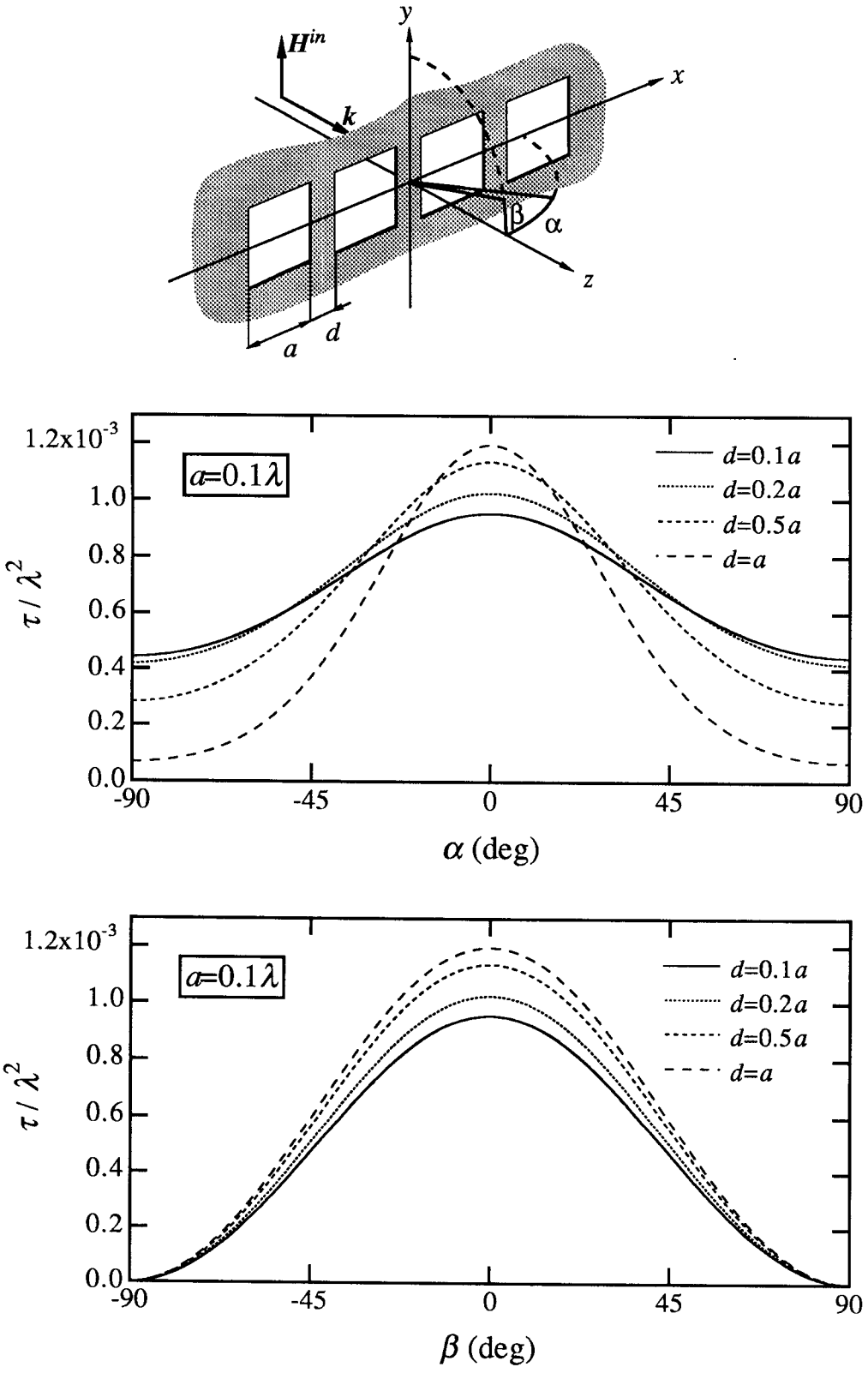

Fig. 10. Transmission cross section of an array of four apertures oriented along the x-axis. Normal incidence and the polarization of the magnetic field parallel to the y-axis. The length of the side of each aperture is 0.1λ.

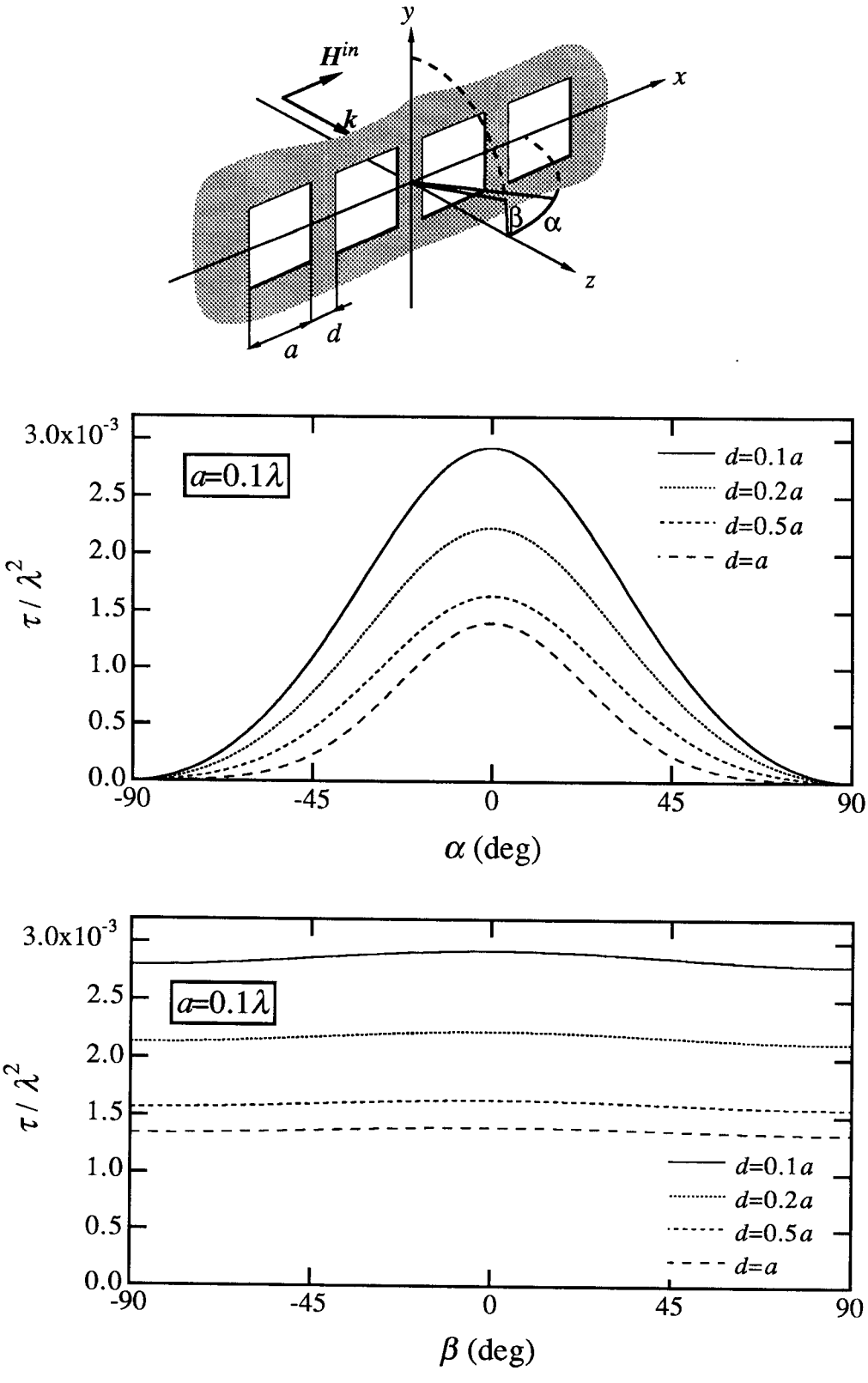

Fig. 11. Transmission cross section of an array of four apertures oriented along the x-axis. Normal incidence and the polarization of the magnetic field parallel to the x-axis. The length of the side of each aperture is 0.1λ.

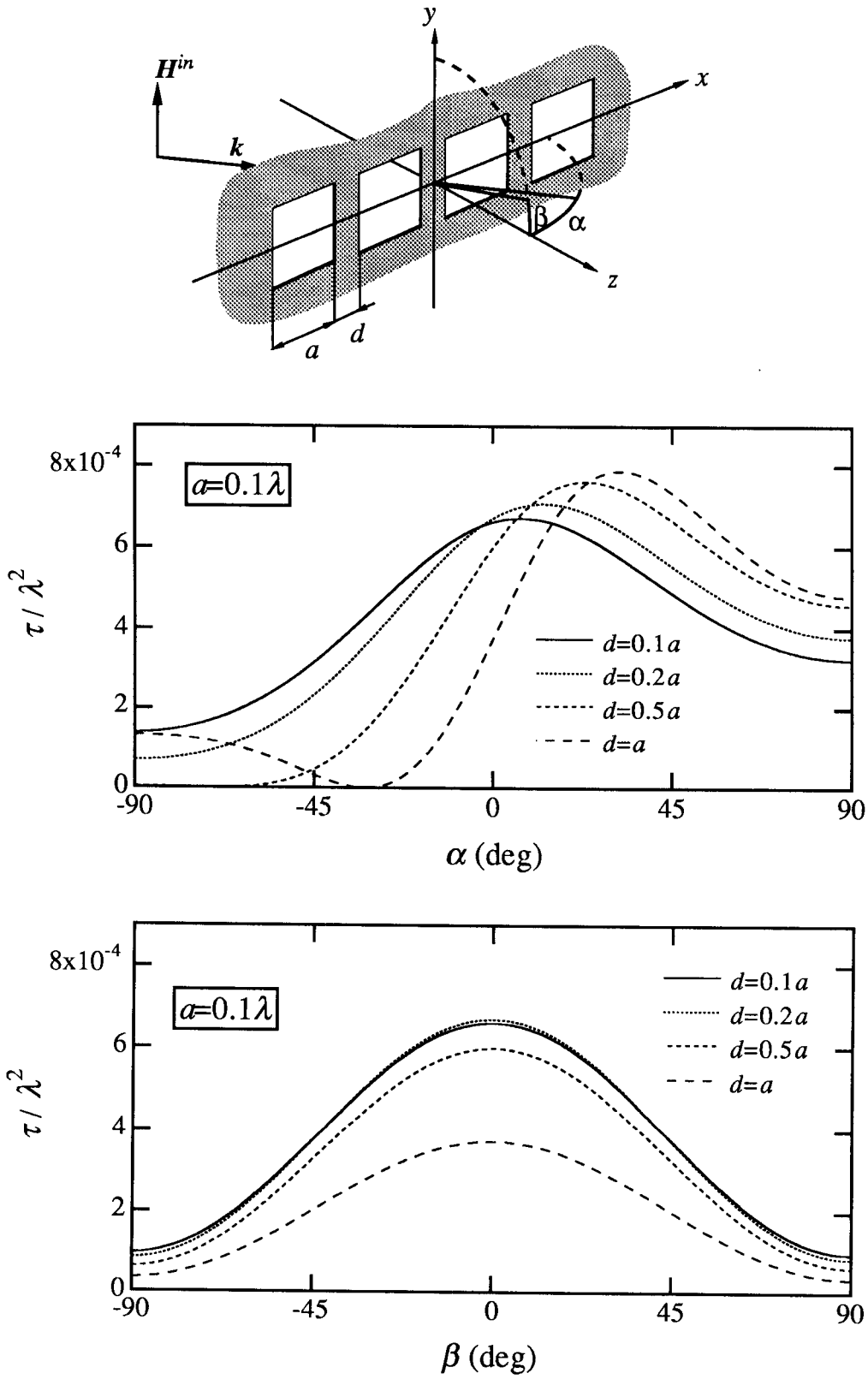

Fig. 12. Transmission cross section of an array of four apertures oriented along the x-axis. The plane of incidence is equal to the x-z-plane and the incidence angle is 45 degrees. The polarization of the magnetic field is parallel to the y-axis. The length of the side of each aperture is 0.1λ.

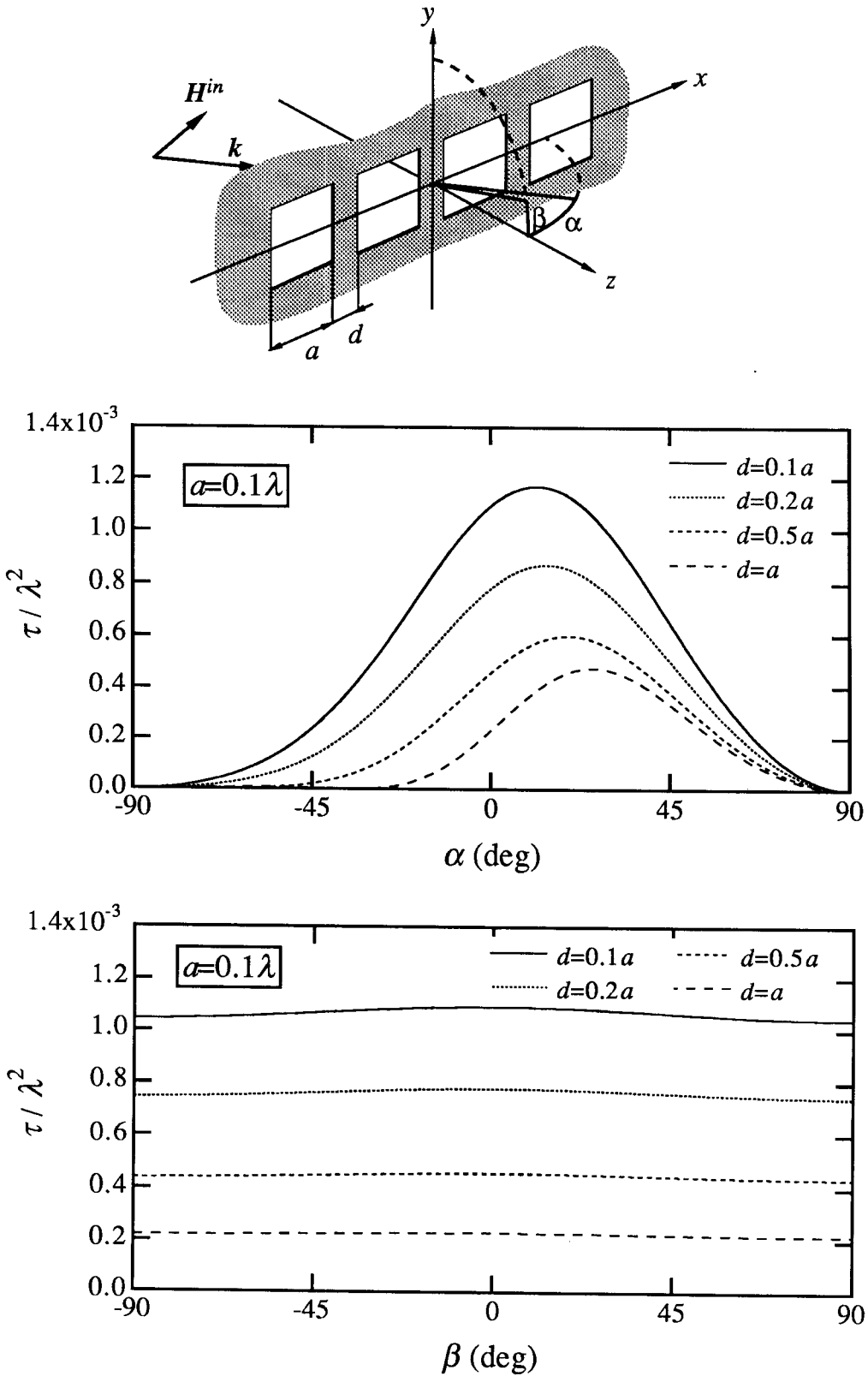

Fig. 13. Transmission cross section of an array of four apertures oriented along the x-axis. The plane of incidence is equal to the x-z-plane and the incidence angle is 45 degrees. The polarization of the magnetic field is perpendicular to the y-axis. The length of the side of each aperture is 0.1λ.

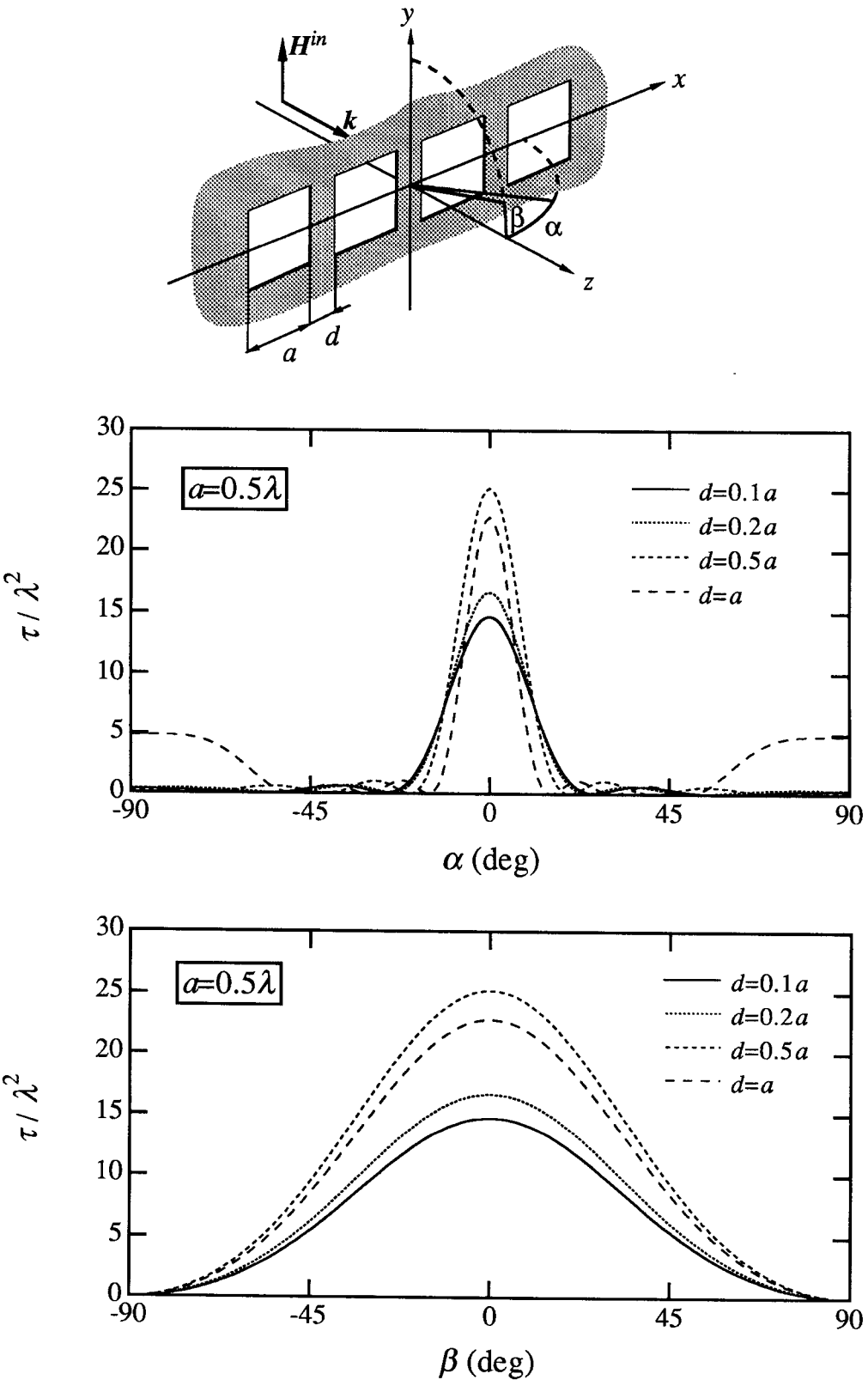

Fig. 14. Transmission cross section of an array of four apertures oriented along the x-axis. Normal incidence and the polarization of the magnetic field parallel to the y-axis. The length of the side of each aperture is 0.5λ.

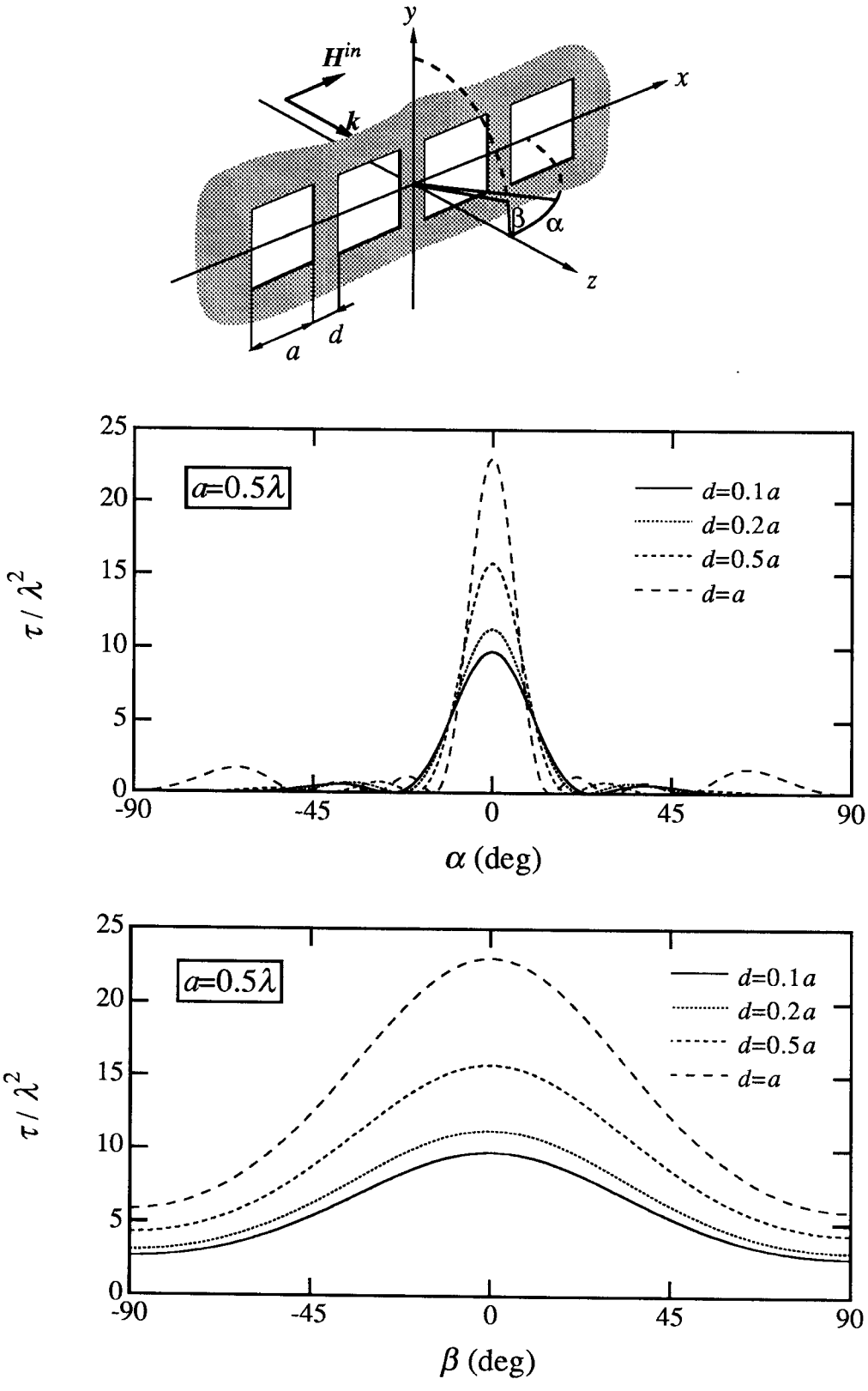

Fig. 15. Transmission cross section of an array of four apertures oriented along the x-axis. Normal incidence and the polarization of the magnetic field parallel to the x-axis. The length of the side of each aperture is 0.5λ.

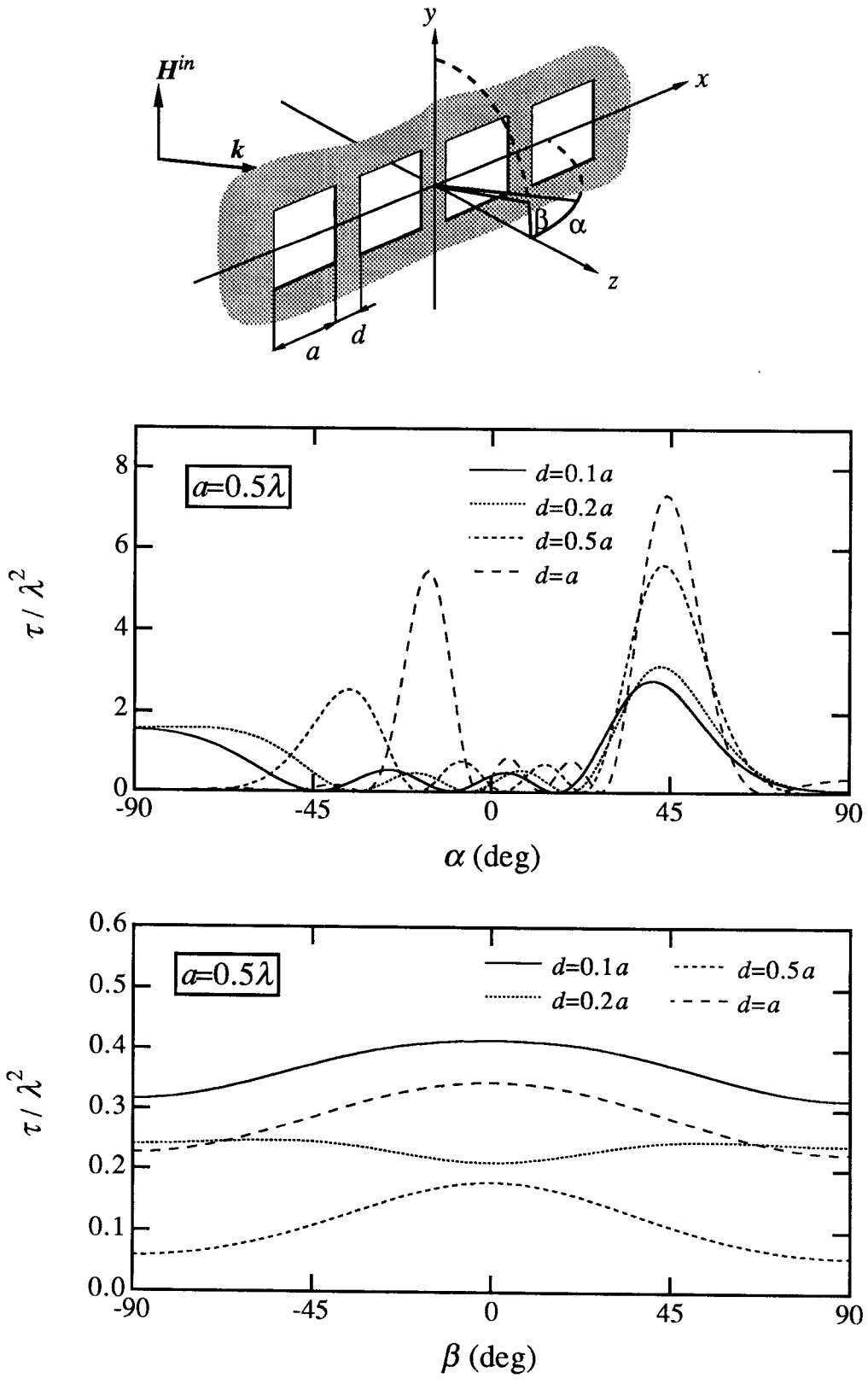

Fig. 16. Transmission cross section of an array of four apertures oriented along the x-axis. The plane of incidence is equal to the x-z-plane and the incidence angle is 45 degrees. The polarization of the magnetic field is parallel to the y-axis. The length of the side of each aperture is 0.5λ.

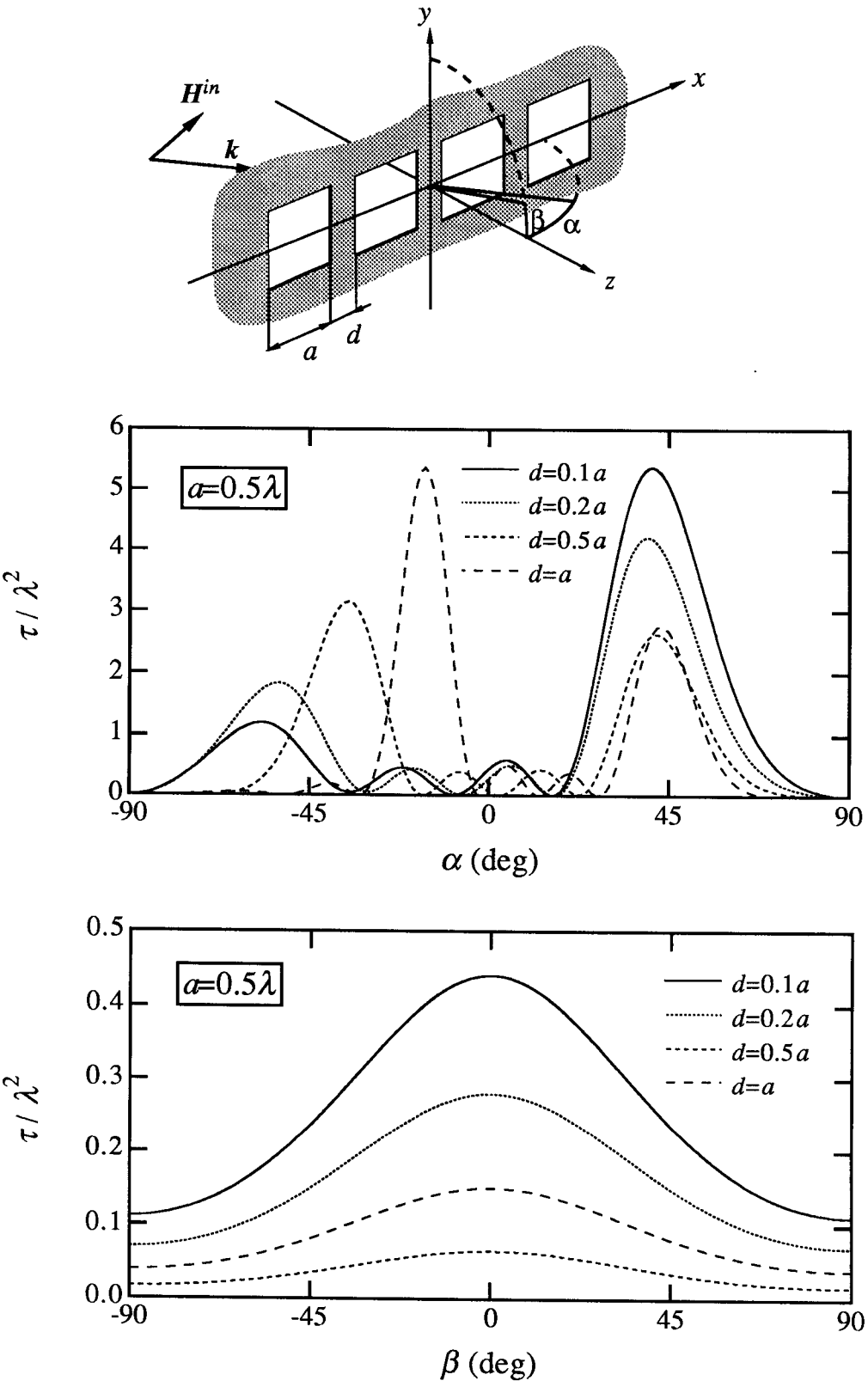

Fig. 17. Transmission cross section of an array of four apertures oriented along the x-axis. The plane of incidence is equal to the x-z-plane and the incidence angle is 45 degrees. The polarization of the magnetic field is perpendicular to the y-axis. The length of the side of each aperture is 0.5λ.

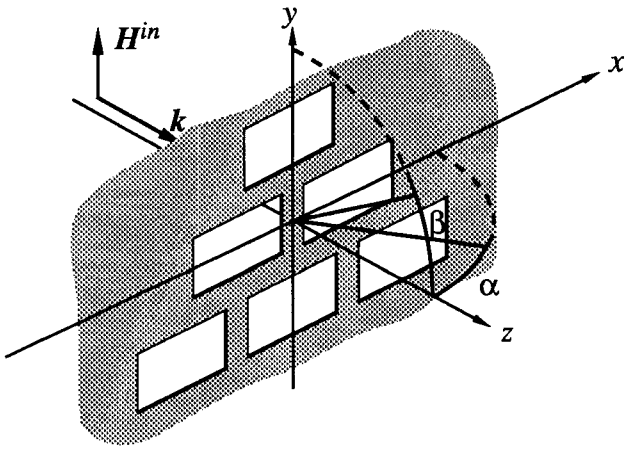

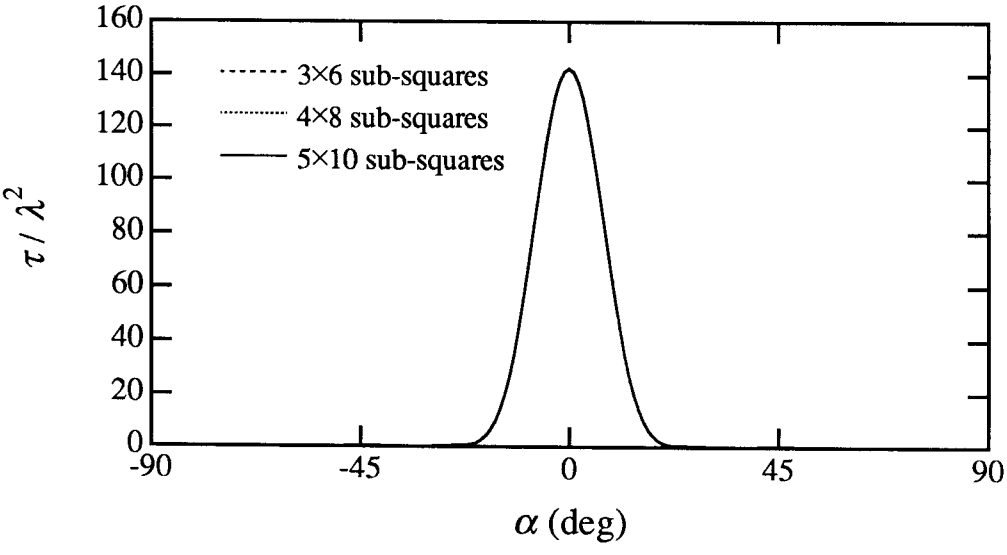

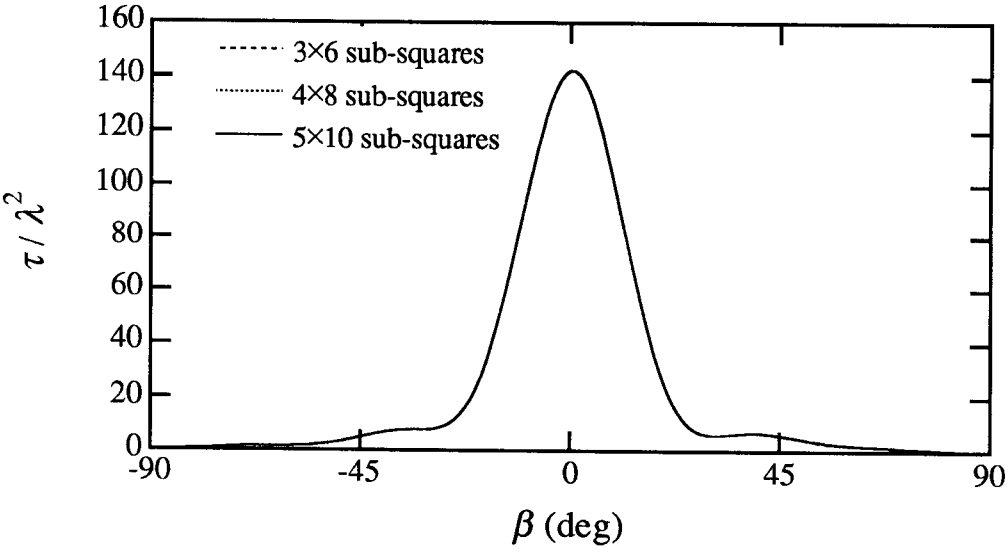

Fig. 18. Transmission cross section of a configuration of six apertures. The size of each aperture is $0.5\lambda \times 1\lambda$ and the distances between the apertures are 0.25λ. The results of three different discretizations of the apertures are illustrated. Normal incidence and polarization of the magnetic field parallel to y-axis.

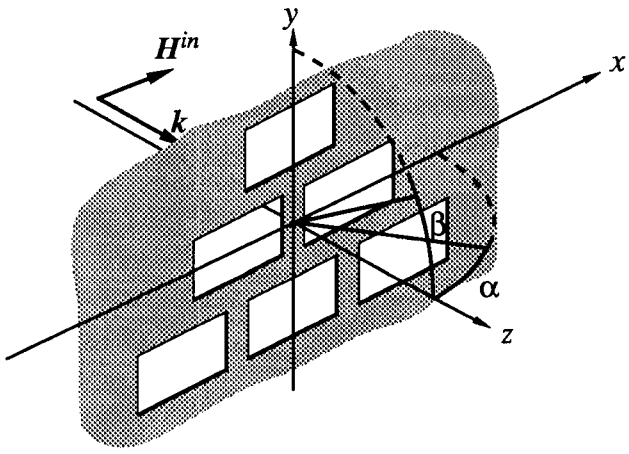

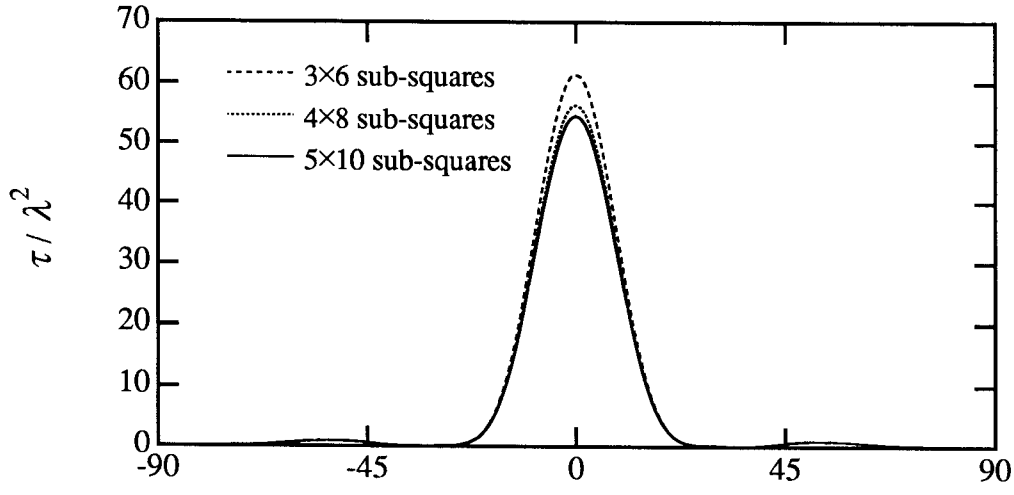

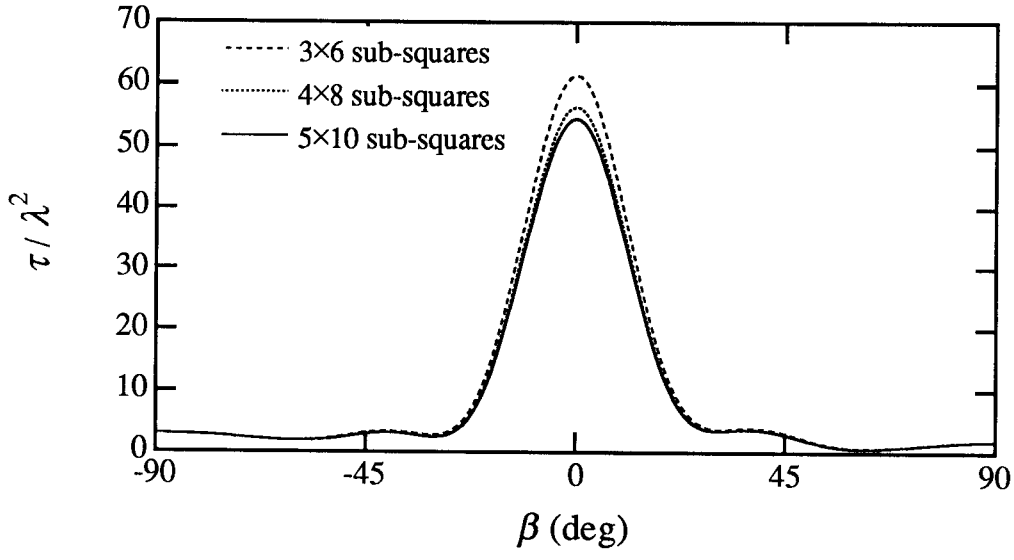

Fig. 19. Transmission cross section of a configuration of six apertures. The size of each aperture is $0.5\lambda \times 1\lambda$ and the distances between the apertures are 0.25λ. The results of three different discretizations of the apertures are illustrated. Normal incidence and polarization of the magnetic field parallel to x-axis.

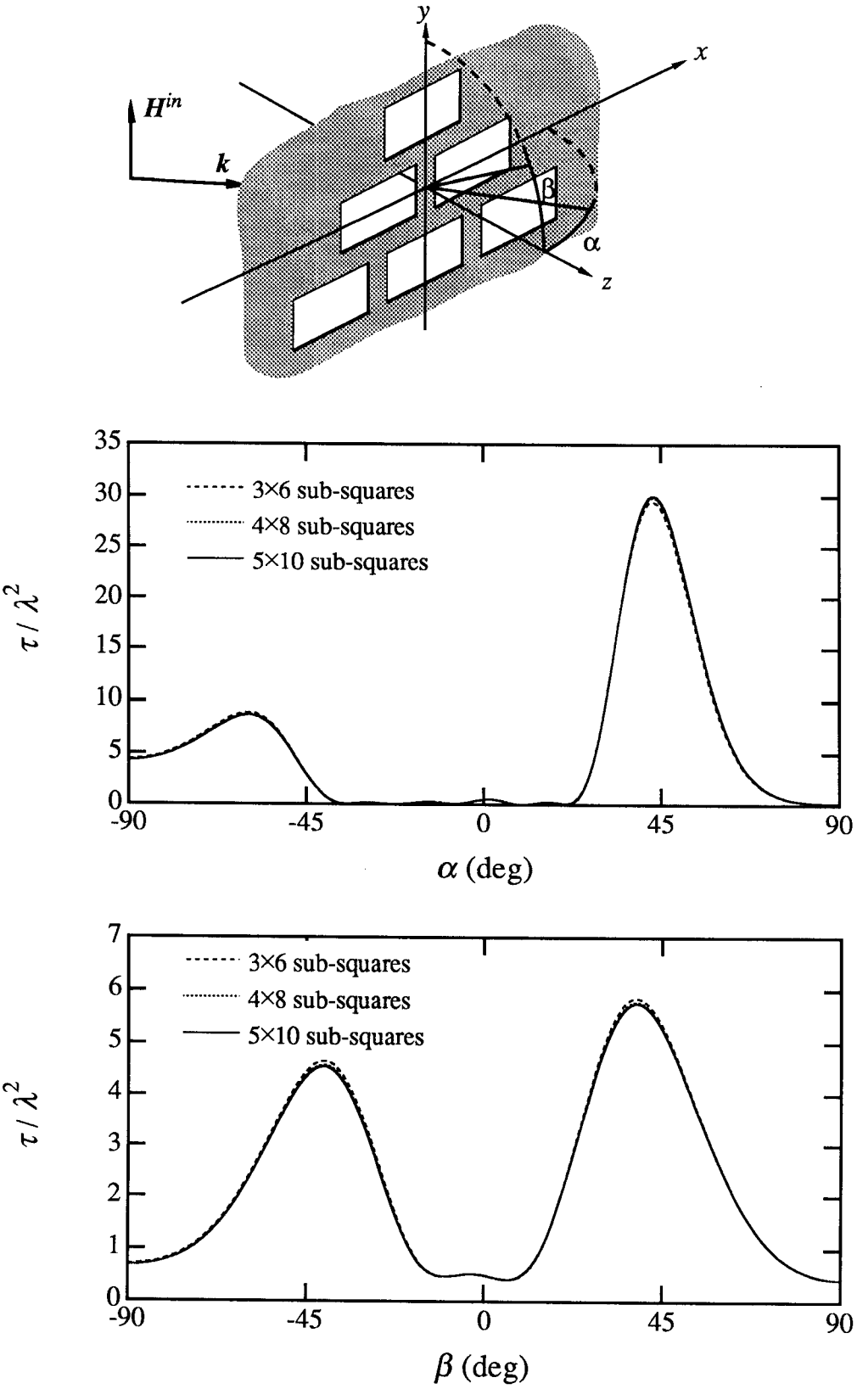

Fig. 20. Transmission cross section of a configuration of six apertures. The size of each aperture is $0.5\lambda \times 1\lambda$ and the distances between the apertures are 0.25λ. The results of three different discretizations of the apertures are illustrated. The plane of incidence is equal to the x-z-plane and the incident angle is 45 degrees. The polarization of the magnetic field is parallel to the y-axis.

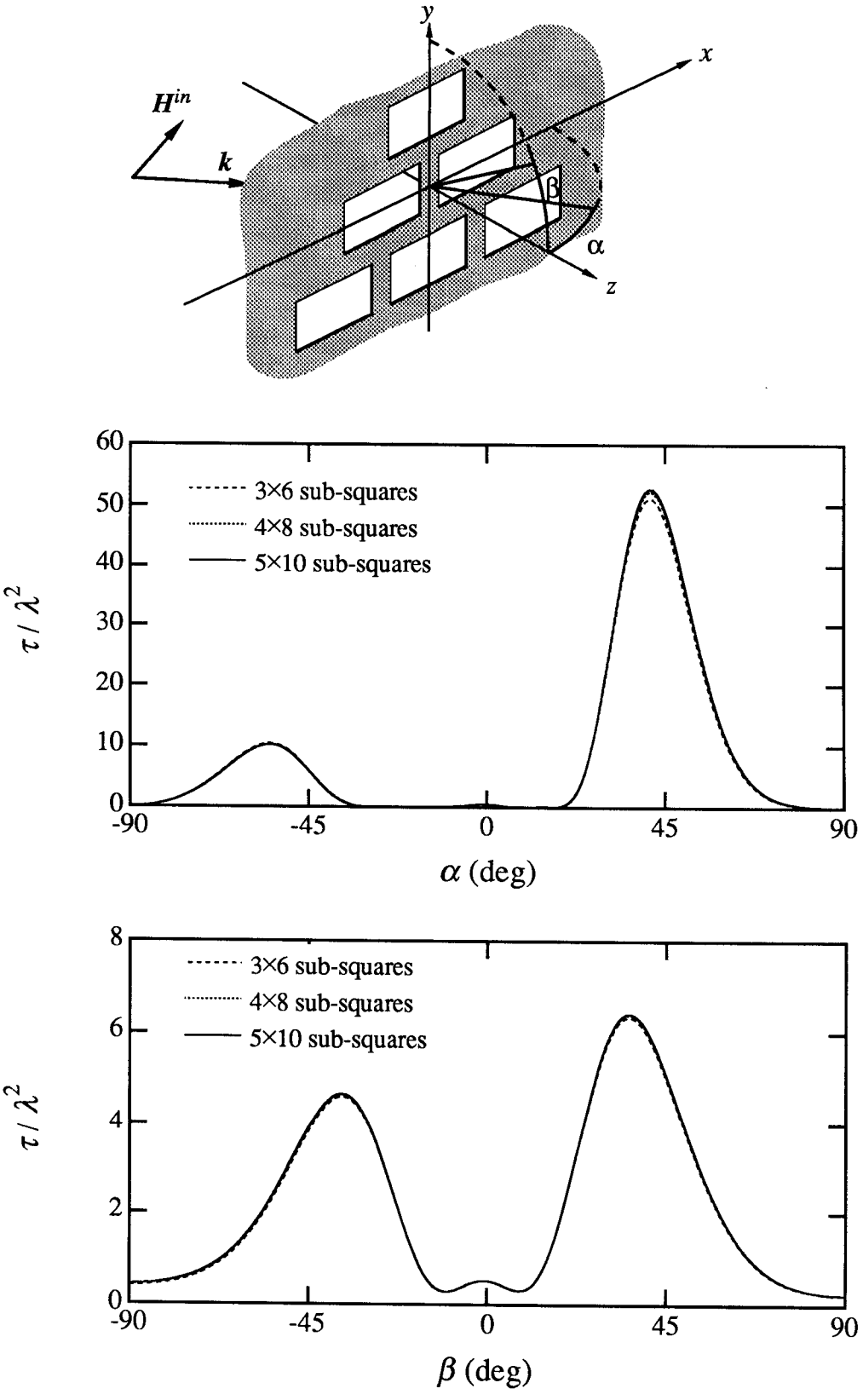

Fig. 21. Transmission cross section of a configuration of six apertures. The size of each aperture is $0.5\lambda \times 1\lambda$ and the distances between the apertures are 0.25λ. The results of three different discretizations of the apertures are illustrated. The plane of incidence is equal to the x-z-plane and the incident angle is 45 degrees. The polarization of the magnetic field is perpendicular to the y-axis.

References

[1] R. B. Kieburtz and A. Ishimaru, "Aperture fields of an array of rectangular apertures," *IRE Trans. Antennas Propagat.*, vol. AP-10, pp. 663-671, Nov. 1962.

[2] M. I. Kontorovich, "Averaged boundary conditions at the surface of a grating with square mesh," *Radio Eng. Elec. Phys.*, vol. 8, pp. 1446-1454, 1963.

[3] C. C. Chen, "Transmission through a conducting screen perforated periodically with apertures," *IEEE Trans. Microwave Theory Tech.*, vol. MTT-18, no. 9, pp. 627-632, Sept. 1970.

[4] D. A. Hill and J. R. Wait, "Electromagnetic scattering of an arbitrary plane wave by two nonintersecting perpendicular wire grids," *Canadian J. Phys.*, vol. 52, pp. 227-237, 1974.

[5] R. F. Harrington, *Field Computation by Moment Methods*, New York, The Macmillan Company, 1968.

[6] R. F. Harrington and J.R. Mautz, "Electromagnetic transmission through an aperture in a conducting plane," *AEÜ*, Band 31, Heft 2, pp. 81-87, 1977.

[7] R. F. Harrington and J. R. Mautz, "A general network formulation for aperture problems," *IEEE Trans. Antennas Propagat.*, vol. AP-24, pp. 870-873, Nov. 1976.

[8] T. K. Sarkar, M. F. Costa, C. L. I and R. F. Harrington, "Electromagnetic transmission through mesh covered apertures and arrays of apertures in a conducting screen," *IEEE Trans. Antennas Propagat.*, vol. AP-32, no. 9, pp. 908-913, Sept. 1984.

[9] W. L. Ko and R. Mittra, "Scattering by a truncated periodic array," *IEEE Trans. Antennas Propagat.*, vol. AP-36, no. 4, pp. 496-503, Apr. 1988.

[10] T. Cwik and R. Mittra, "The effects of the truncation and curvature of periodic surfaces: A strip grating," *IEEE Trans. Antennas Propagat.*, vol. AP-36, no. 5, pp. 612-622, May 1988.

[11] R. Kastner and R. Mittra, "Iterative analysis of finite-sized planar frequency selective surfaces with rectangular patches or perforations," *IEEE Trans. Antennas Propagat.*, vol. AP-35, no. 4, pp. 372-377, Apr. 1987.

[12] L. Gurel and W. C. Chew, "Recursive algorithms for calculating the scattering from *N* strips or patches," *IEEE Trans. Antennas Propagat.*, vol. AP-38, no. 4, pp. 507-515, Apr. 1990.

[13] R. De Smedt and J. Van Bladel, "Magnetic polarizability of some small apertures," *IEEE Trans. Antennas Propagat.*, vol. AP-28, no. 5, pp. 703-707, Sept. 1980.

[14] R. De Smedt, "Low frequency scattering through an aperture in a rigid screen - some numerical results," *J. Sound and Vibration*, vol. 75 no. 3, pp. 371-386, 1981.

[15] T. Andersson, "Moment-method calculations of scattering by a square plate using singular basis functions and multipole expansions," *J. Electro. Waves Applic.* (In Press).

[16] C. M. Butler, Y. Rahmat-Samii and R. Mittra, "Electromagnetic penetration through apertures in conducting surfaces," *IEEE Trans. Antennas Propagat.*, vol. AP-26, no. 1, pp. 82-93, Jan. 1978.

[17] R. F. Harrington, *Time-Harmonic Electromagnetic Fields*, New York, The Macmillan Company, 1961.

[18] D. Colton and R. Kress, *Integral equations methods in scattering theory*, New York, John Wiley & Sons, 1983.

[19] J. Van Bladel, *Singular Electromagnetic Fields and Sources*, Oxford, Clarendon Press, 1991.

[20] T. Andersson, "Method of moments and the use of multipole expansion," *J. Electro. Waves Applic.*, vol. 5, no. 11. pp. 1237-1257, 1991.

[21] A. Boström, G. Kristensson and S. Ström, "Transformation properties of plane, spherical, and cylindrical scalar and vector wave functions," in *Field Representations and Introduction to Scattering*; Eds. V. V. Varadan, A. Lakhtakia and V. K. Varadan, vol. 1, Amsterdam, North Holland, 1991.